Gait Classification With Gait Inherent Attribute Identification From Ankle's Kinematics

Yogesh Singh and Vineet Vashista, *Member, IEEE*

***Abstract*— The human ankle joint interacts with the environment during ambulation to provide mobility and maintain stability. This association changes depending on the different gait patterns of day-to-day life. In this study, we investigated this interaction and extracted kinematic information to classify human walking mode into upstairs, downstairs, treadmill, overground and stationary in real-time using a single-DoF IMU axis. The proposed algorithm's uniqueness is twofold - it encompasses components of the ankle's biomechanics and subject-specificity through the extraction of inherent walking attributes and user calibration. The performance analysis with forty healthy participants (mean age: 26.8 $\pm$ 5.6 years yielded an accuracy of 89.57% and 87.55% in the left and right sensors, respectively. The study, also, portrays the implementation of heuristics to combine predictions from sensors at both feet to yield a single conclusive decision with better performance measures. The simplicity yet reliability of the algorithm in healthy participants and the observation of inherent multimodal walking features, similar to young adults, in elderly participants through a case study, demonstrate our proposed algorithm's potential as a high-level automatic switching framework in robotic gait interventions for multimodal walking.**

***Index Terms*— Ankle kinematics, multimodal walking, gait classification.**

I. Introduction

THE improvement and restoration of the gait performance while ambulating in daily living conditions, which involves activities of ascending/descending stairs and overground walking, has been an important aspect of the robotic rehabilitation community [1]–[3]. Walking in a controlled laboratory setting does not represent a realistic scenario of the real world where users involve multiple walking modes [1], [2]. Walking in multimodal conditions with the trivial interventions of aerobic exercises, strength training, and treadmill walking, stroke, older adults (aged 71 years and above) and Parkinson's Disease patients have shown generalizability and transference effects of gait training into unsupervised walking [4], [5].

Manuscript received September 28, 2021; revised February 28, 2022; accepted March 16, 2022. Date of publication March 24, 2022; date of current version April 5, 2022. This work was supported in part by the Department of Science and Technology, India, under Grant DST/INSPIRE/04/2015/001077. The work of Yogesh Singh was supported by the Prime Minister Research Fellows (PMRF) Fellowship. *(Corresponding author: Vineet Vashista.)*

This work involved human subjects in its research. Approval of all ethical and experimental procedures and protocols was granted by the Indian Institute of Technology Gandhinagar Ethics Committee under Identifier No. IEC/2019-20/4/VV/036.

The authors are with the Human-Centered Robotics Laboratory, IIT Gandhinagar, Gandhinagar, Gujarat 382355, India (e-mail: yogesh.singh@iitgn.ac.in; vineet.vashista@iitgn.ac.in).

Digital Object Identifier 10.1109/TNSRE.2022.3162035

There are abundant gait studies that have shown successful robotic gait interventions in neuromuscular disorder patient groups in single walking mode involving treadmill [6]–[8], overground [9]–[11], or stairs walking [12]–[14]. In these interventions, an important decision process of determining the duration, magnitude, and activation instance of the externally applied assistive forces requires elements of subject-specificity and gait adaptability. To achieve these intervention objectives, different kinds of adaptive and data-driven algorithms have been developed utilizing single [15], [16] or multiple sensors [17], [18].

In multimodal walking, each mode has a specific biomechanical requirement, and the same intervention cannot be applied across all walking modes. In Kang *et al.* [1], different walking mode-specific hip-joint moment trajectories were implemented to design multimodal gait interventions with the controller manually switching its intervention type. Ankle-joint moment trajectory being different in each walking mode, a ground reaction-based model for the ankle moment control strategy was designed for multimodal gait intervention [2]. For effective and successful implementation of multimodal interventions in activities of daily living, there is a need to automatically switch from one walking mode to another for specific gait intervention.

The current modalities of classifying multimodal walking use a data-driven approach of gait models or machine learning techniques [18]–[28]. The classification algorithms based on support vector machine [19], [21], [22], neural networks [21], [23], fuzzy logic [24], [25], k-nearest neighbors [18], [20], decision tree [21], Bayesian networks [26], [27], and Gaussian Mixture Model [28] have been developed providing accuracies from 77.3% to 97.6%. These methods rely on a large dataset for training the model offline, post-processing algorithms, or utilizing multiple sensorial inputs for walking mode classification, which have been identified to add computation load and processing speed constraints [2], [27]. Further, such approaches have been projected as black box models [27], where the biomechanical significance of different walking modes remains unknown. Therefore, there is a need for developing classification algorithms with gait adaptability and subject specificity that promotes smooth real-time intervention applications while transitioning between different modes of daily living activities.

Walking is the outcome of interlimb coordination and synchronized joint movements [29]. During multimodal walking, the multi-limb movements are altered to meet the need for specific walking mode. The rhythmic flow and the repetitiveness

of walking is one of the striking inherent and common features across walking modes [30]. In this work, we aim to exploit the kinematic repetitiveness of lower limb movements to develop algorithms for multimodal walking classification. Further, we investigate the repetitive nature of the ankle kinematics to extract inherent attributes specific to different modes of multimodal walking.

In this study, a single sensor and single-DoF input-based real-time classification algorithm is developed to detect walking modes of upstairs, downstairs, treadmill, overground, and stationary. As the shank and the foot segments are connected with the ankle joint, the shank was chosen to place the inertial sensor to acquire repetitive gyroscopic angular velocity in different walking modes. The algorithm was evaluated with performance measures in multimodal locomotion testing with forty healthy individuals. We hypothesized that (i) investigating ankle joint motion in different walking modes will elicit inherent features to classify the states of multimodal locomotion; and (ii) with key feature identification, a single-DoF repetitive signal acquisition will yield high-performance measures. A case study with two elderly participants was conducted to demonstrate the applicability of the proposed classification algorithm for future utilization in targeted population groups.

II. Method

A. Subject Participation and Experimental Protocol

Forty healthy subjects volunteered to take part in the study. Participants were informed about the research procedure and signed a written consent approved by the Indian Institute of Technology Gandhinagar Ethics Committee (Identifier Number: IEC/2019-20/4/VV/036). None of the participants reported any gait disorder and could walk comfortably without any assistance. Research assistants obtained information about the demographic variables of the participants (mean age: 26.8 $\pm$ 5.6 years; height: 168.5 $\pm$ 15.7 cm; weight: 76.8 $\pm$ 10.2 kgs; 32 right footed and 8 left footed; 26 males and 14 females). Exclusion criteria for the study involved ambulation inability due to neuromuscular disorder.

The validity of the classifier algorithm was tested by experimenting with 40 healthy participants. The experimental paradigm was designed to contain all five walking modes – upstairs, downstairs, treadmill, overground and stationary - in one session. The participants wore the sensor units that were connected to the smartphone application over WiFi. The experiment comprised of two phases – the calibration and the trial phase. The calibration was done prior to the trial phase for 20 seconds during which the participants walked overground at a comfortable speed. The initiation of both phases was controlled by the smartphone application. The participant followed experimental protocol in the order - upstairs (US, 5 stairs), downstairs (DS, 5 stairs), US (5 stairs), overground (OG, $\approx$ 100m) and treadmill (TM, 1 minute) with 10 sec of stationary (S) in between two walking states except when transitioning from US to OG, as shown in Fig. 1A. The trial took an average of 176.47 $\pm$ 8.91 seconds to complete for a single participant. The research assistants walked alongside the participant to guide them through the walking passage back to the laboratory.

B. Sensor System Overview

1) Hardware: A sensor system with portable and wearable capabilities was designed for this study as shown in Fig. 1A-B. The current system contains two shank units, one for each foot, and a smartphone application for providing real-time feedback of the predicted walking state and user's other gait characteristics. Each shank unit contains a raspberry pi 3A+ single-board computer, 9-axis inertial measurement unit (IMU, SparkFun 9-DoF Razor M0), and a 3800 mAh Li-ion battery to power the unit. The range of IMU's accelerometer and the gyroscope axes were configured at $\pm$ 2g and $\pm$ 2000°/s, respectively.

2) Unit Placement: The components of each sensor unit were mounted on an elastic velcro brace with a 3D printed housing on top. The assembled unit was worn as an ankle bracelet around the lower end of the shank closer to the ankle joint. The positive local Z-axis of the IMU was adjusted to point outwards from the body in the left-to-right direction (approximately aligning with the mediolateral walking axis), Fig. 1B. The alignment of IMU's X and Y axes to any biomechanical walking axis does not bear significance as these DoFs were not used in the algorithm. However, to be consistent in the protocol, the X-axis was approximately aligned perpendicularly to the tibia and the Y-axis along the shank's longitudinal axis.

3) Communication Protocol: The IMU communicates with raspberry pi 3A+ using a Universal Asynchronous Receiver-Transmitter (UART) protocol. The IMU data acquisition and the gait classification and characterization were performed at 100 Hz. The smartphone and the shank units were connected to the same hosted network over WiFi, Fig. 1B. The smartphone was configured as a server and the shank units as clients. A Transmission Control Protocol (TCP) socket was created at a pre-defined idle port number to facilitate communication between the server and the clients. To start using the system, the smartphone application sent separate triggers to both the shank units simultaneously via TCP packets over WiFi for calibrating algorithm parameters and starting the experiment. The clients, then, respond with the necessary gait data of fixed byte length for streaming. The streaming rate on the smartphone application was configured at 100 Hz.

4) Smartphone Application: An user-interactive application was developed using the Python-based Kivy platform. The application utilizes the host smartphone's WiFi to create a server and connects with the client shank units for wireless data transfer using the TCP socket framework. The application streams the classified walking mode states, IMU's local z-axis gyroscope values, events in a walking cycle, walking frequency, and time elapsed from both the shank units. It also provides controls to start the calibration and the actual trial.

C. Gait Classification

The finite state machine diagram in Fig. 2 depicts the information flow of various parameters to classify walking modes.

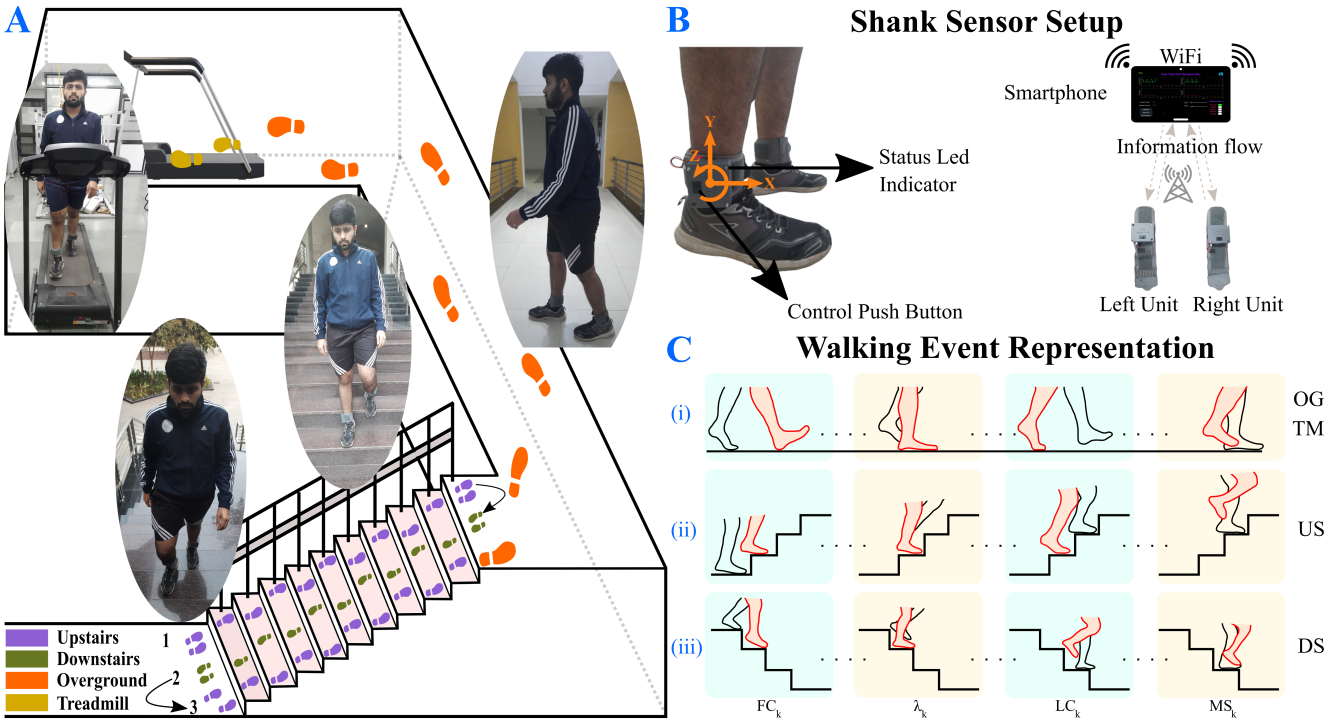

Fig. 1. A) Image illustrating experimental protocol adopted for testing the classifier algorithm: upstairs (10 steps) → downstairs (10 steps) → upstairs (10 steps) → overground (≈100m with two left turns) → treadmill walking (60s). The participant depicted agreed to the use of their image. B) Both the shank sensor systems are shown that predicts walking states in real-time. The sensors connect with the smartphone over the same hosted WiFi network and provide feedback onto a custom designed smartphone application using transmission control protocol (TCP). C) Representation of FC_k, λ_k, LC_k, and MS_k events in the four walking states of (i) overground (OG), treadmill (TM), (ii) upstairs (US), and (iii) downstairs (DS). FC_k corresponds to heel-strike in OG and TM states whereas LC_k refers to toe-off in OG and TM. For normal walking on stairs, LC_k may correspond to toe-off. λ_k event occurs between FC_k and LC_k when the contralateral foot is swinging.

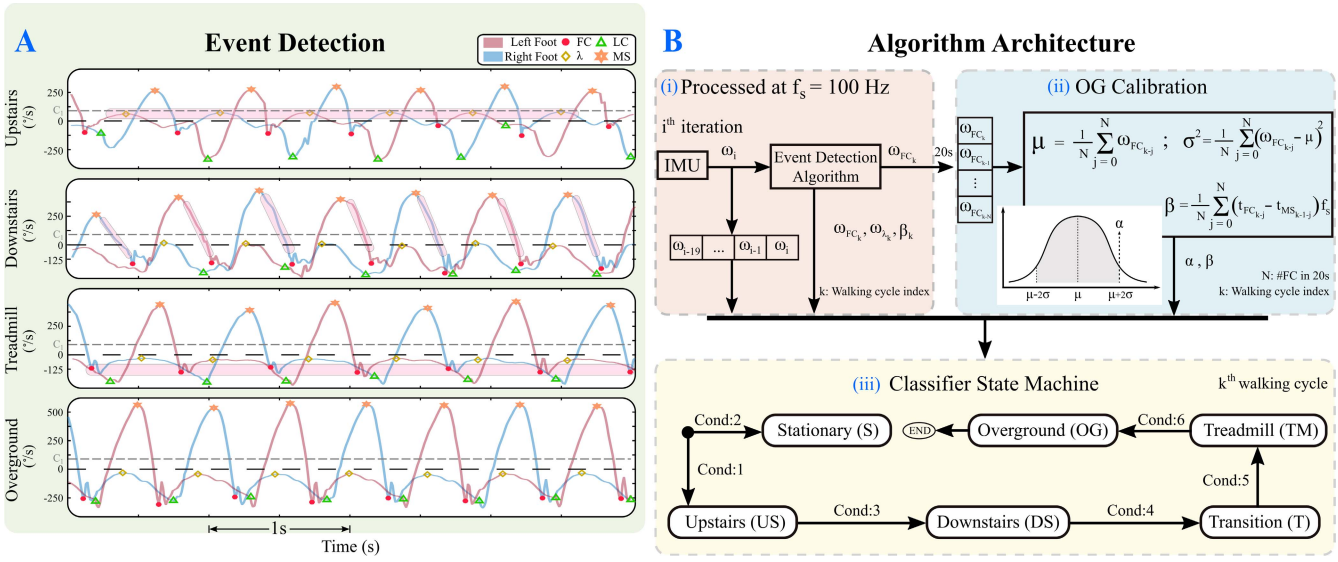

Fig. 2. A) The results of events detection algorithm for the different walking modes are depicted. All the walking modes show unique features represented in the pink enclosed box. The events of foot contact (FC), last contact (LC), classifier decision peak (λ), and mid-swing (MS) remains prominent among all walking modes. C_1 is a sensor calibrated constant used for differentiating FC valley from the LC valley. B) The state machine diagram for the gait classification implemented at each sensor unit. (i) The mediolateral gyroscope values, ω, are accessed from the IMU each iteration at 100 Hz and are fed to the event detection algorithm that outputs the four walking events every k^{th} walking cycle. (ii) The calibration algorithm computes two calibrated parameters, α_{cal} and β_{cal} over the overground walking. (iii) The classifier algorithm, Algorithm 2, is invoked once every walking cycle at λ_k-peak that predicts {ζ, T, S} walking modes. Until the detection of the next λ_k-peak event, the previous state of the classifier is maintained.

It involves three layers of algorithm which are processed at different frequency rate - (a) the event detection algorithm, Fig. 2B(i), runs at 100 Hz and give outputs once every walking cycle (at the user's walking frequency), (b) the calibration algorithm, Fig. 2B(ii), runs once at the end of 20s over-ground calibration prior to the experimental trial, and (c) the

classification algorithm for the walking states (ζ := US, DS, TM, OG), runs at the user's walking frequency, Fig. 2B(iii). All three layers of the algorithm work on the single-DoF, local z-axis, gyroscope values and its operated derivatives, refer Fig. 2B, thereby reducing processing complexity and power consumption.

1) Walking Event Detection: The event detection algorithm recognizes major events in every k^{th} walking cycle - First Contact (FC_k), Last Contact (LC_k), and Mid-Swing (MS_k) for different walking patterns in ζ, refer Fig. 1C. Another critical event, λ_k-peak, is detected that invokes the gait classification algorithm.

The FC_k is defined as the event when the foot makes contact with the ground to initiate the k^{th} walking cycle. It corresponds to Heel-Strikes (HSs) when in OG or TM walking, as shown in Fig. 1C(i). The LC_k is the event at which the foot lifts-off the ground providing propulsion to move forward. The LC_k events are the Toe-Offs (TOs) in OG and TM walking, refer Fig. 1C(i). For normal walking on stairs, the LC_ks may also correspond to TOs as the body has a tendency to move forward during walking and shifts the body weight to the leading foot via trailing foot's TO, refer Fig. 1C(ii, iii). The MS_k is defined as the event when the swinging leg passes the contralateral leg in stance phase with both legs side-by-side as depicted in Fig. 1C(i-iii). The λ_k-peak is defined as the event that occurs between FC_k and LC_k as a peak of the gyroscope's mediolateral axis waveform, ω, and the contralateral leg is swinging as shown Fig. 1C(i-iii). Therefore, the sequence of event detection is FC_k (valley), λ_k (peak), LC_k (valley), and MS_k (peak) from ω waveform. To ensure that the two valleys are differentiated accurately, the former valley (FC_k) occurs after MS_{k-1} when the ω profile has crossed a positive sensor calibrated value, (C_1), twice as in line 6 Algorithm 1. The latter valley (LC_k) occurs after λ_k-peak as in line 13 of Algorithm 1. Similarly, the two peaks (λ_k and MS_k) are distinguished with a sequential search of these events. The value of C_1 was set through a pilot test phase where the ω waveform nature in swing phase was observed for a comfortable walking speed range of 1.5 to 3 kmph. The C_1 magnitude 90.123°/sec is the minimum angular velocity that the shank surpasses twice in the swing phase - the first time while the ankle is plantarflexed (ω waveform going up) and the second time when the ankle is dorsiflexed (ω waveform coming down), see Fig. 2A. The decimal number of C_1 is kept to three places to ensure the equality condition never hold in line 4 of Algorithm 1 considering that the ω signal acquired from the gyroscope is upto two decimal places.

2) Calibration: The walking style of every individual is unique resulting in different parametric nature of key events in a walking cycle. The calibration phase provides two important features for real-time assessment in gait classification, thus, preserves the subject-specific component of the algorithm. The calibration trial requires the participant to walk overground at a comfortable speed for 20 seconds once before the experimental trial. At the end of 20 seconds, the algorithm computes the participant-specific baseline values denoted by α_{cal} and β_{cal}. Let N be the number of gait cycles in the calibration phase then μ and σ denote the mean and standard deviation of ω_{FC_k} with k = 1, 2, ... N, respectively, see Fig. 2B(ii). The α_{cal} is statistically defined as two standard deviations above the mean, $\mu + 2\sigma$, which is the upper limit of the 95.45% normal distribution of ω_{FC_k}, refer Fig. 2B(ii). β_{cal} is the mean of the number of data points between MS_{k-1} and FC_k - an indicator to the slope of the ω waveform between the two events, refer Fig. 2B(ii).

3) Classification: The distinguishing features of the ω waveform among ζ states used in the current work for healthy gait are highlighted in Fig. 2A. In US, there is a clear distinction from other walking states. The algorithm classifies US when the λ_k-peak takes positive ω values, as in line 4 Algorithm 2. The DS is predicted when the slope of ω

Algorithm 1: Event Detection

1 ***Initialization:***
$C_1 \leftarrow 90.123$ ▷ Sensor calibrated value
$f_s \leftarrow 100$ ▷ Sampling frequency (Hz)
$\mu_1, \mu_2 \leftarrow 0.4, 0.66$ ▷ Waveform constants
$\omega_{FC_k}, \omega_{\lambda_k}, \omega_{LC_k}, \omega_{MS_k} \leftarrow$ NaN $C_{FC} \leftarrow 0$
while $\omega_i \leftarrow Gyroscope_{Z-axis}$ **do**
2 A[1:20] $\leftarrow \omega_i, \omega_{i-1}, \ldots\omega_{i-19}$ ▷ Stack buffer A
function detectEvent()
3 **if** $(\omega_i - C_1)(\omega_{i-1} - C_1) < 0$ **then**
4 C_{FC}++;
5 **if** $C_{FC} == 2$ **then**
6 **if** *valleyFound()* < 0 **then**
7 FC_k detected; $C_{FC} \leftarrow 0$;
8 **if** $\mu_1\omega_{FC} \leq \omega_i \leq C_1$ **then**
9 **if** *peakFound()* < 0 **&&** $FC_k \neq \{\}$ **then**
10 λ_k-peak detected;
11 **if** $\omega_i \leq \mu_2$ **then**
12 **if** *valleyFound()* < 0 **&&** $\lambda_k \neq \{\}$ **then**
13 LC_k detected;
14 **if** *peakFound()* > 0 **&&** $LC_k \neq \{\}$ **then**
15 MS_k detected;

Algorithm 2: Gait Classification

1 ***Initialization:***
$C_2 \leftarrow 3$ $CS \leftarrow$ OG ▷ default OG state
function stateClassify()
2 **if** $\lambda_k \neq \{\}$ **then**
3 **if** $\omega_{\lambda_k} > 0$ **then**
4 $CS_k \leftarrow$ US ▷ US detected
5 **if** $\beta_k > \beta_{cal}$ **then**
6 $CS_k \leftarrow$ DS ▷ DS detected
7 **if** $\omega_{FC_k} > \alpha$ **&&** $CS_{k-1} \neq TM$ **then**
8 $CS_k \leftarrow$ T ▷ T detected
9 **if** $\omega_{FC_k} > \alpha$ **&&** $CS_{k-1} \neq (DS \parallel US)$ **then**
10 $CS_k \leftarrow$ TM ▷ TM detected
11 **if** $\omega_{FC_k} \leq \alpha$ **then**
12 $CS_k \leftarrow$ OG ▷ OG detected
13 **if** $abs(A_{max} - A_{min}) < C_2$ **then**
14 $CS_k \leftarrow$ S ▷ S detected

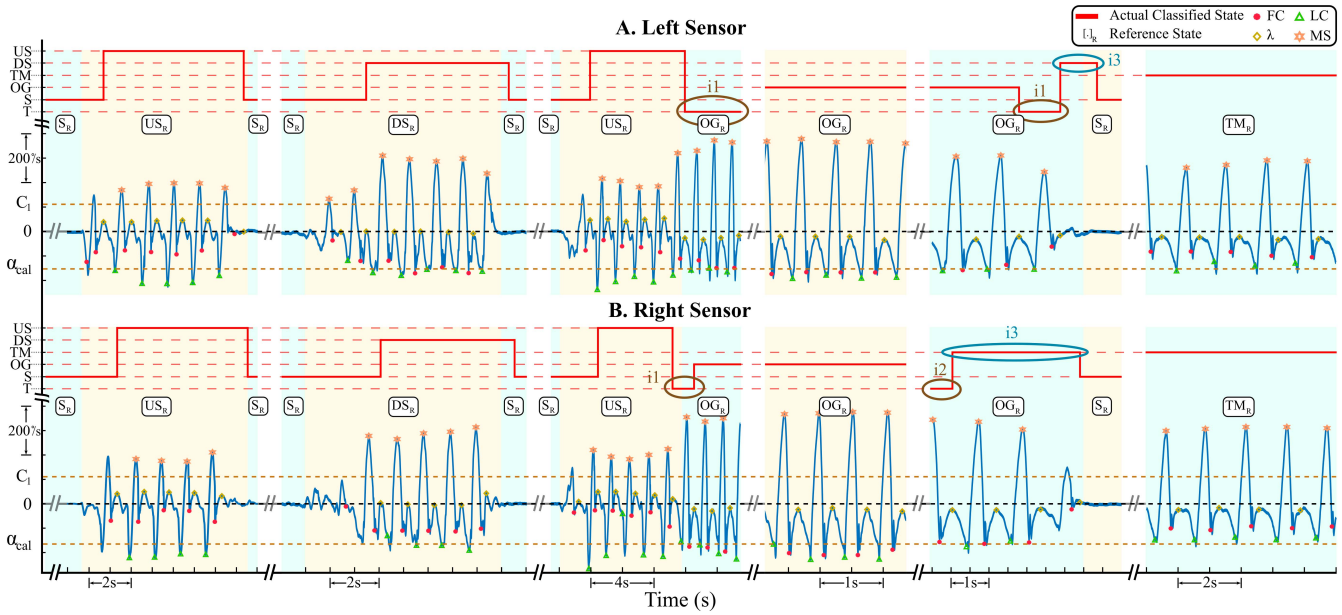

Fig. 3. The plot shows the result of the proposed walking mode classification algorithm in real-time for a representative participant on both the sensor units - left (A) and right (B) shanks. The sensor calibrated value, C_1, and participant calibrated parameter, α_{cal}, are also depicted for the representative participant. The real-time detection of walking events - first contact (FC_k), λ_k-peak, last contact (LC_k), and mid-swing (MS_k) are shown on each sensor's gyroscope waveform along local z-axis. The actual (predicted) states are depicted in red plots whereas the reference (ground truth) state is shown in alternated blue- and yellow-shaded regions with a $[.]_R$.

waveform between the MS_{k-1} and FC_k events decreases gradually compared to other walking states where the decline is steep, coded in line 6 Algorithm 2. OG is declared whenever ω_{FC_k} value goes below the calibrated α_{cal} as in line 12 of Algorithm 2 whereas in TM, the ω_{FC_k} lies above α_{cal}, accounted in line 10 Algorithm 2. The defining features of US and DS are mutually exclusive, thereby, an intrinsic feature of these states. However, the differentiating feature of OG/TM is not mutually exclusive with US and DS, i.e., the ω_{FC_k} in US and DS may be above α_{cal}. Therefore, the classification algorithm is structured in an if-statement ladder such that it searches for the US and DS first before exploring the TM and OG states, refer Algorithm 2. Additionally, the algorithm uses a holding state, referred as the Transition (T) state, to improve its reliability. The S state is determined outside the if-statement structure by examining the peak-to-peak ω values in the $(A_{1\times 20})$ buffer to be within C_2 range indicating a flattened ω waveform as in line 14 of Algorithm 2. The buffer size 20 of A was decided through pilot testing with the objective to keep the computation cost low from storing previous values of ω signal. Keeping the size to be as minimum as one-fifth of the sample acquisition frequency ($f_s = 100$ Hz) ensures that the S state is detected without comprising the computation load. Overall, the algorithm classifies the walking modes into $\{\zeta, \text{T}, \text{S}\}$ predicted states at the λ_k-peak once every walking cycle. The λ_k-peak event is used as a triggering event to activate the classification algorithm, Algorithm 1, as depicted the algorithm architecture in Fig. 2B.

III. Performance Evaluation and Results

The real-time classified walking mode states were stored and extracted successfully for performance evaluation. Figure 3 shows a real-time gait classification made by the algorithm (red plots) for both feet (left, Fig. 3A, and right, Fig. 3B) for a representative participant. The red plot varies between the $\{\zeta, \text{T}, \text{S}\}$ predicted states. The reference state for each timeline is shown in $[x]_R$ subscripted labels in alternating blue- and yellow-colored bands; where $x \in \{\zeta, \text{S}\}$. The sensor constant C_1 and each foot calibrated α_{cal} values are depicted in Fig. 3.

A. Evaluation Metrics

The performance evaluation was done by constructing the confusion matrix and estimating precision, recall, F-measure, and accuracy parameters. The ground truth (reference) and predicted (actual) classified states during walking were examined at the λ_k-peak. To compare the stationary part of the experimental trial, S events were defined at one-second intervals. The set containing both the λ_k-peak and S events is referred to as E (evaluation) events. The ground truth states at E events were computed at the λ_k-peak event as the predictions of $\{\zeta, \text{T}, \text{S}\}$ states were also performed at the same event, keeping the number of samples equal in predicted and ground truth conditions. The ground truth states were specified in post-processing as per the experimental protocol. The actual classified state from the algorithm was taken from the real-time classification performed by the sensor units. Although the classification algorithm also predicts a transition (T) state during the experiment, as discussed in Section II-3, there is no corresponding reference state to compare the predicted T state.

Consequently, a 5×5 Confusion Matrix (CM) was generated considering all E events, as shown in Table I - CM column. CM is a table with actual and predicted states appearing as rows and columns, respectively. Each (i, j) value cross-references the instances of j^{th} predicted state with its i^{th}

TABLE I

CONFUSION MATRIX (CM, LEFT COLUMN) AND PERFORMANCE MATRIX (PM, RIGHT COLUMN) OF 30 PARTICIPANTS FOR DIFFERENT CASES OF (i) LEFT SENSOR (LS), (ii) RIGHT SENSOR (RS), (iii) HEURISTIC-1 (ϕ_{H1}), AND (iv) HEURISTIC-2 (ϕ_{H1}) SHOWN BELOW

	Confusion Matrix (CM)*							Performance Matrix (PM, in %)					
(i) Left Sensor	**Reference, Prediction**	**S**	**US**	**DS**	**OG**	**TM**	**T**	**Measure, States**	**S**	**US**	**DS**	**OG**	**TM**
	S	1592	5	0	11	3	7	**Precision**	94.65	91.62	79.21	95.94	95.29
	US	21	328	6	0	0	43	**Recall**	98.39	82.41	70.85	82.54	90.48
	DS	9	0	141	6	16	27	**F1-Score**	96.48	86.77	74.80	88.73	92.82
	OG	11	25	8	1087	57	129						
	TM	49	0	23	29	1539	61	**Accuracy**			89.57		
(ii) Right Sensor	**Reference, Prediction**	**S**	**US**	**DS**	**OG**	**TM**	**T**	**Measure, States**	**S**	**US**	**DS**	**OG**	**TM**
	S	1604	8	6	9	4	6	**Precision**	95.25	86.67	74.05	96.06	97.11
	US	22	273	8	0	0	84	**Recall**	97.98	70.54	50.00	80.08	91.43
	DS	13	0	97	11	17	56	**F1-Score**	96.60	77.78	59.69	87.34	94.19
	OG	9	34	6	1049	25	187						
	TM	36	0	14	23	1547	72	**Accuracy**			87.55		
(iii) Heuristics - 1	**Reference, Prediction**	**S**	**US**	**DS**	**OG**	**TM**	**T**	**Measure, States**	**S**	**US**	**DS**	**OG**	**TM**
	S	1451	4	3	7	5	167	**Precision**	94.53	81.05	83.53	97.40	98.19
	US	26	201	2	0	0	158	**Recall**	88.64	51.94	36.60	68.55	84.06
	DS	11	0	71	4	10	98	**F1-Score**	91.49	63.31	50.90	80.47	90.58
	OG	0	43	0	898	11	358						
	TM	47	0	9	13	1413	199	**Accuracy**			77.44		
(iv) Heuristics - 2	**Reference, Prediction**	**S**	**US**	**DS**	**OG**	**TM**	**T**	**Measure, States**	**S**	**US**	**DS**	**OG**	**TM**
	S	1593	6	6	12	15	5	**Precision**	92.78	85.29	80.73	95.93	95.72
	US	43	319	3	0	0	22	**Recall**	97.31	82.43	79.90	84.50	90.48
	DS	6	0	155	9	10	14	**F1-Score**	94.99	83.84	80.31	89.85	93.03
	OG	7	49	5	1107	43	99						
	TM	68	0	23	26	1521	43	**Accuracy**			90.13		

*Each sample in the Confusion Matrix corresponds to a single E event which comprises both the λ_k-peak event (occurring once in a walking cycle) and the stationary (S) event.

reference state. Therefore, the diagonal of CM is the instances of predicted states in agreement with the ground truth. The performance parameters of precision, recall, and F1-Score [31] for an 'X' state of walking mode and overall accuracy were determined from the CM as shown below. TP, FP, and FN denote the True Positive, False Positive, and False Negative, respectively.

$$\text{Precision}_X = \frac{\text{TP}_X}{\text{TP}_X + \text{FP}_X} \tag{1}$$

$$\text{Recall}_X = \frac{\text{TP}_X}{\text{TP}_X + \text{FN}_X} \tag{2}$$

$$\text{F1-Score}_X = \frac{2 * \text{Precision}_X * \text{Recall}_X}{\text{Precision}_X + \text{Recall}_X} \tag{3}$$

$$\text{Accuracy} = \frac{\sum \text{TP}_X}{\text{Total Samples}} \tag{4}$$

The holding state, T, has been appended as an additional column in CM to represent incorrect estimation with respect to the ground truth. Thereby, while computing performance measures from CM, the number of predicted T states was accounted for in the computation of recall and accuracy. By definition, the precision of individual states does not consider the instances of T state predictions.

B. Gait Classification Heuristics

As per the implemented scheme, both sensor units predicted the walking state independently during the experimental trial. Let ϕ_L and ϕ_R denote the independent classified walking mode states from the left and right sensor units respectively, such that, $\phi_L(n)$, $\phi_R(n) \in \{\zeta, \text{T}, \text{S}\}$ at n^{th} instance of E events. As both units are used for classification, it is reasonable to combine the decision and provide a single conclusive classified state. Therefore, various heuristics can be developed to this effect. In this work, we considered two straightforward heuristics. The rules of the heuristics were applied in the offline post-processing analysis and they were defined as below.

Heuristic 1 (ϕ_{H1}): was defined as the retention of the state in case of same predictions by both sensor units otherwise T state was assigned. Therefore:

$$\phi_{H1}(n) = \begin{cases} \phi(n), & \text{if } \phi_L(n) = \phi_R(n) = \phi(n) \\ T, & \text{otherwise} \end{cases} \tag{5}$$

Heuristic 2 (ϕ_{H2}): was defined as the assignment of the previous classified state in case of different decisions by the sensor units otherwise the same state was retained.

$$\phi_{H2}(n) = \begin{cases} \phi(n), & \text{if } \phi_L(n) = \phi_R(n) \\ \phi(n-1), & \text{otherwise} \end{cases} \tag{6}$$

In the above heuristics, the classified states ϕ_L and ϕ_R were compared at the E events of the two sensor units. Due to the temporal shift in the occurrence of the E events depending upon the gait initiating foot, the selection of $\phi(n)$ and $\phi(n-1)$ was randomized between the two sensor units to prevent bias due to selection order.

C. Results

Figure 3 shows both sensors' evolution of ω waveform during the experimental protocol with real-time predicted classified states (red plot) for a representative participant. The algorithm retains or changes the predicted state value at the λ_k-peak event. The ground truth label is assigned at each λ_k-peak in post-data processing. There is a temporal shift in the λ_k-peak between the two sensors depending upon the gait initiating foot, thereby, a phase shift in the prediction of new walking states. The T state is observed to be predicted during gait changes from US to OG, OG to S (i1 encircled regions) and left turn in right sensor (i2) whereas incorrect state prediction occurs in the i3 region.

The algorithm's performance analysis in the Left Sensor (LS) and Right Sensor (RS), shown in Table I(i-ii) PM, yielded high accuracy of 89.57% and 87.55%, respectively. LS and RS had similar precision in S, OG, and TM states with $94.65\%_{LS}$ and $95.25\%_{RS}$ in S, $95.94\%_{LS}$ and $96.06\%_{RS}$ in OG, and $95.29\%_{LS}$ and $97.11\%_{RS}$ in TM. The S, OG, and TM states showed similar recall measures in LS and RS having $98.39\%_{LS}$ and $97.98\%_{RS}$ in S, $82.54\%_{LS}$ and $80.08\%_{RS}$ in OG, and $90.48\%_{LS}$ and $91.43\%_{RS}$ in TM. However, LS had a higher recall in both US and DS compared to RS yielding $82.41\%_{LS}$ and $70.54\%_{RS}$ in US, and $70.85\%_{LS}$ and $50.00\%_{RS}$ in DS. Consequently, LS and RS showed similar F1-Score values of 96.48_{LS} and 96.60_{RS} in S, 88.73_{LS} and 87.34_{RS} in OG, and 92.82_{LS} and 94.19_{RS} in TM. The difference in F1-Score between LS and RS was large with higher values in LS - 86.77_{LS} and 77.78_{RS} in US and 74.80_{LS} and 59.69_{RS} in DS.

The application of heuristic–1 showed an accuracy of 77.44% - a decrease in accuracy compared to 89.57% and 87.55% in LS and RS, respectively, refer Table I(iii) - PM column. The precision achieved was 94.53%, 81.05%, 83.53%, 97.40%, and 98.19% in S, US, DS, OG, and TM states, respectively, being fairly similar to LS and RS. However, the recall obtained was 88.64%, 51.94%, 36.60%, 68.55%, and 84.06% in S, US, DS, OG, and TM states, respectively, which was reduced compared to LS and RS scores discussed above. It is expected as H1 declares a T state when both sensors differ in their predictions. Therefore, the T state column in Table I(iii) - CM has high values compared to LS and RS. With similar precision but poor recall, the H1 has reduced F1- Score values of 91.49 in S, 63.31 in US, 50.90 in DS, 80.47 in OG, and 90.58 in TM compared to LS and RS as shown in Table I(i-iii).

The performance results of implementing heuristic-2 are shown in Table I(iv) - PM column. The accuracy obtained is 90.13% which was a slight increment from LS (89.57%) and RS (87.55%). The precision was 92.78%, 85.29%, 80.73%, 95.93%, and 95.72% in S, US, DS, OG, and TM states, respectively, which is either an intermediate value or closer to the minimum value between LS and RS precision scores. The recall improved for the DS and OG states at 79.90% and 84.50%, respectively, with an in-between or improved recall for the S, US, and TM compared to LS and RS at 97.31%, 82.43%, and 90.48%, respectively. The H2 implementation retains the best of both LS and RS predictions with improvement in the recall measures. Consequently, the F1-measure was improved for the DS and OG states at 80.31 and 89.85, respectively, and similar scores in S, US, and TM with 94.99, 83.84, and 93.03, respectively. The T state column entries in CM for H2 were also the lowest among the ζ states compared to LS, RS, and H1. The diagonal entries for the US, DS, and OG states in CM were highest among all cases indicating the highest true positive value, i.e., instances of reference and prediction states coinciding for H2.

IV. Discussion and Conclusion

The problem of identifying multimodal walking intention carries significant value in the field of rehabilitation through robotic interventions. Human movements have a greater degree of redundancy and dexterity to ambulate, resulting in variations in their gait characteristics to maintain stability and mobility [32], [33]. An important contributor to this flexibility in locomotion can be attributed to the human ankle joint which regularly interacts with the environment [32]. In this study, we showcased the ability of the ankle's kinematics to successfully classify human walking modes into stationary, upstairs, downstairs, treadmill, and overground walking patterns using a single-DoF gyroscope axis in real-time.

The proposed classification algorithm, independently, in each sensor unit has shown its efficacy to classify forty healthy human walking modes with reasonably high-performance measures. With the single-DoF gyroscope axis, the algorithm was able to give high accuracy of 89.57% and 87.55% in the left and right sensors, respectively. These results are noteworthy compared to other existing gait classification studies. Many studies have shown better classification accuracy but with more sensor inputs and feature selection [18], [22], [34]. Studies with a single sensor have also presented walking mode classification using random forest (accuracy of 76.1% and 86.29% with machine learning and subject-based model, respectively) [35], k-nearest neighbor [20], fuzzy logic [25], decision tree with signal processing [36] for different patterns of level walking, ascending and descending stairs with sit and stand activities. In contrast, the current study employs a single sensor to extract unique features intrinsic to the walking states that greatly reduced the reliance on multiple feature extraction models using signal processing techniques compared to existing works. This makes the proposed classification algorithm compatible to use for the real-time robotic interventions in multimodal walking where externally applied assistive forces need to adapt to the walking mode.

Moreover, this novel contribution forms a white box approach to incorrect classification rationale by promoting collaboration between the algorithm and biomechanical aspects of walking which has been projected as a useful autonomous and reliable framework for assistive gait intervention [27].

For instance, the dataset reveals a significant difference in the recall measure of left and right sensor units primarily as a consequence of high transition predictions in right sensor during upstairs, downstairs, and overground states. Further inspection revealed that left turns in the paradigm induced more transitions in right sensors in overground suggesting the tendency of the left foot to initiate the turn naturally with the lagging contralateral right foot coming along later to complete the turning trajectory. This difference in the two sensor units showcases the foot specificness of the algorithm which could be useful for rehabilitation purposes.

The current work demonstrates the implications of implementing heuristics to enhance the algorithm's performance by holistically combining individual sensor decisions. Further, there is merit to developing more heuristics to optimize the algorithm's performance depending upon its application and the participant group. Among the applied heuristics 1 and 2, the latter combined the best of both sensor units' performance to yield an accuracy of 90.13%. Moreover, although a single sensor can be used independently for healthy individuals, incorporating heuristics for a patient group can show significantly improved performance by combining the classification states empirically from both the sensor units.

The central aspect of this work has been to capture the ankle's kinematics using a single sensor for gait classification. Therefore, the placement is critical to gather the ankle's biomechanics with the single sensor and was deliberately chosen at the lower shank above the ankle joint. The IMU being mounted on the shank senses the ankle's rollover kinematics in the stance phase of gait. Using this sensor placement approach, it enabled the classification of walking states using inherent feature identification with a single-DoF gyroscope axis. With other studies, the gait classification required more feature selection, sensors or multi-DoF IMU, temporal gait information at first contact, last contact and gait phase [20], [25], [35], [36]. The placement of IMU on the foot segment would miss the ankle kinematics in the stance phase due to flat foot condition, though, such placement has found applications in pedestrian localization and spatial gait measurements [37], [38], [40]–[45].

The classifier decision peak, λ_k-peak, plays a crucial role in the algorithm's structure as a trigger event to predict a walking state once every gait cycle. The λ_k-peak was specifically chosen because of its distinct characteristics. The sign of the ω waveform at the λ_k-peak is an important identifier for the upstairs walking mode. At λ_k-peak, all sufficient input conditions for the prediction are available to be fed into the classification algorithm. Moreover, the λ_k-peak is observed when the gyroscope sensor is attached to the shank as in this current study and not when placed on the foot [46], [47].

From the adopted approach of placing the sensor at the shank, the upstairs and downstairs states depicted their inherent features as mutually exclusive to other walking states. During upstairs progression, the shank rocks forward after the first contact and then backward post heel-off about the ankle joint in stance phase resulting in both dorsiflexion and plantarflexion. This is in contrast to other walking states where the shank rotates only forward about the ankle in stance causing dorsiflexion [32], [33]. In downstairs, the sensor gathers the downslope inclination of the stairs that causes the first contact to occur at lower ground level than the previous first contact. It results in a gradual decrease in the ω waveform after mid-swing making this behavior unique compared to flat overground walking, treadmill or upstairs. The significant moment is produced in dorsiflexors with similar ankle joint power in overground than treadmill walking during the loading response [48]. The presented work utilized this fact kinematically, which meant smaller angular velocity at first contact in overground than the treadmill at comfortable walking speed.

The approach adopted, in this work, is subject-specific algorithm development. In contrast to machine learning models where training model needs access to the large dataset for reliable performance, the proposed algorithm uses calibration phase to tune itself to specific participants. The walking attributes shown in this work are intrinsic to a particular state, however, the calibrated parameters for state decision-making are subject-specific. In the current work, the experiment trial was conducted in immediate subsequent to the calibration phase that estimated two unique statistical parameters of shank angular velocity at first contact and its slope between mid-swing and first contact.

The study has certain limitations. The current experimental protocol did not include the targeted speed variation range like slow or fast ambulating speed across walking modes - participants were advised to walk at their preferred comfortable speed. Future studies can test multiple aspects of the proposed algorithm such as inter-rater reliability, scattered walking patterns, multi-day study for home use. In future work, new classification states of slope walking and sit-to-stand activities can also be added.

The intended application of this work is for use in rehabilitation for the patient groups involving daily walking activities on flat surfaces. Classification of walking modes is essential for the effective administration of intervention through robotic devices. Together with the gait temporal data from key walking events, the proposed classification algorithm can help clinicians observe gait changes and be informed of users' gait performance under different walking modes. It could, further, be potentially useful in identifying subjects exhibiting variable or deviated gait characteristics from healthy population groups. Our approach to formulating holding T state could be effective in providing adaptive ways for the robotic controller to tune its parameter during transitioning gait periods to optimize performance in subsequent phases.

A. Case Study

A study was conducted with two healthy older adults (65 and 69 years). The participants wore the sensors on both shanks and performed the calibration protocol followed by locomotion tasks of overground walking (OG $\approx$ 90 m), downstairs (DS, 24 steps), upstairs (US, 24 steps), and stationary (S) for 10 seconds. The values of C_1 and buffer size of A array were kept the same as with the young adult participants. The testing protocol was performed on a daily commute route with left and right turns, a flat walking surface for overground and a staircase for stairs walking, and no treadmill walking mode.

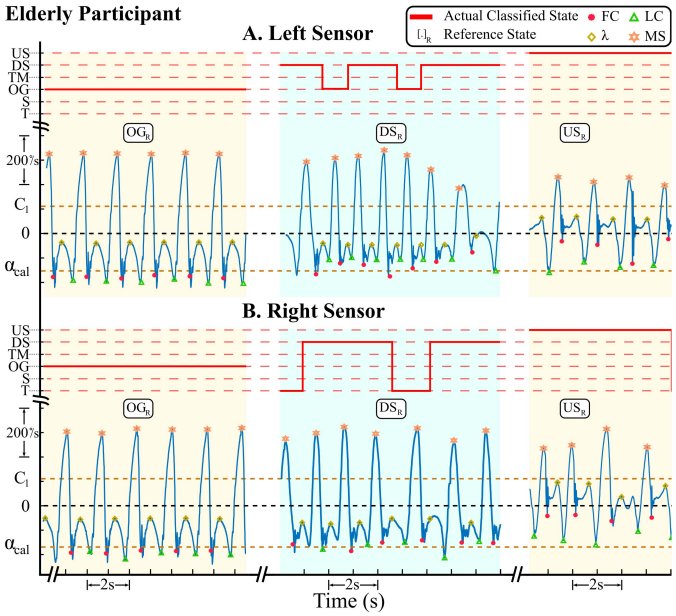

Fig. 4. The plot shows the ω waveform for a representative elderly participant from both sensors. The real-time walking mode classification is depicted in the figure with a red line plot, and the ground truth is shown with the yellow and blue alternating shaded region denoted by $[.]_R$. The walking events of First Contact, λ-peak, Toe-Off, and Mid-Swing are detected by the algorithm in the ω waveform variation in a walking cycle.

For the first elderly participant, the classification algorithm correctly predicted 21 out of 24 DS states, 20 out of 24 US states, 81 out of 86 OG states, 9 out of 11 S states, and 9 transition states. The prediction for the second elderly participant was 20 out of 24 DS states, 22 out of 24 US states, 84 out of 93 OG states, 10 out of 12 S states, and 11 transition states. Fig. 4 shows the plot of the real-time walking mode classification of a representative elderly participant for the OG, DS, and US states.

The results from the case study convey the importance and the future applicability of our proposed algorithm. Walking is a rhythmic and coordinated interlimb movement containing inherent features that occurs repetitively. In multimodal walking, the distinct inherent features separating each walking mode in young adults are also prevalent in elderly adults because the identified inherent feature relates to the biomechanics requirement of the particular walking mode. Irrespective of the young or older adults, both groups show similar repetitive behavior of the ω waveform nature under multimodal walking. In future work, testing with more older adults and other targeted population groups can be performed to make our proposed algorithm beneficial for their robotic gait intervention as an automatic switching framework in daily living activities of multimodal walking.

REFERENCES

[1] I. Kang, D. D. Molinaro, S. Duggal, Y. Chen, P. Kunapuli, and A. J. Young, "Real-time gait phase estimation for robotic hip exoskeleton control during multimodal locomotion," *IEEE Robot. Autom. Lett.*, vol. 6, no. 2, pp. 3491–3497, Apr. 2021.

[2] S. S. P. A. Bishe, T. Nguyen, Y. Fang, and Z. F. Lerner, "Adaptive ankle exoskeleton control: Validation across diverse walking conditions," *IEEE Trans. Med. Robot. Bionics*, vol. 3, no. 3, pp. 801–812, Aug. 2021.

[3] S. Zhou, Z. Zhao, X. Liu, X. Zhu, and J. Chen, "A real-time assistance control strategy for active knee exoskeleton," in *Proc. Chin. Intell. Syst. Conf.* Singapore: Springer, 2022, pp. 621–633.

[4] M. G. Pellicer, A. C. Lusar, J. M. Casanovas, and B.-C.-S. Ferrer, "Effectiveness of a multimodal exercise rehabilitation program on walking capacity and functionality after a stroke," *J. Exercise Rehabil.*, vol. 13, no. 6, pp. 666–675, Dec. 2017.

[5] J. Gudlaugsson *et al.*, "Effects of a 6-month multimodal training intervention on retention of functional fitness in older adults: A randomized-controlled cross-over design," *Int. J. Behav. Nutrition Phys. Activity*, vol. 9, no. 1, pp. 1–11, Dec. 2012.

[6] A. Bishnoi, R. Lee, Y. Hu, and M. Hernandez, "Effect of treadmill interventions on spatiotemporal gait parameters in adults with neurological disorders: Systematic review and meta-analysis of randomized controlled trials," *Arch. Phys. Med. Rehabil.*, vol. 102, no. 10, p. e112, Oct. 2021.

[7] A. C. Dzewaltowski, E. A. Hedrick, T. J. Leutzinger, L. E. Remski, and A. B. Rosen, "The effect of split-belt treadmill interventions on step length asymmetry in individuals poststroke: A systematic review with meta-analysis," *Neurorehabilitation Neural Repair*, vol. 35, no. 7, pp. 563–575, Jul. 2021.

[8] M. Pohl, G. Rockstroh, S. Rückriem, G. Mrass, and J. Mehrholz, "Immediate effects of speed-dependent treadmill training on gait parameters in early Parkinson's disease," *Arch. Phys. Med. Rehabil.*, vol. 84, no. 12, pp. 1760–1766, 2003.

[9] A. J. Del-Ama, Á. Gil-Agudo, J. L. Pons, and J. C. Moreno, "Hybrid gait training with an overground robot for people with incomplete spinal cord injury: A pilot study," *Frontiers Hum. Neurosci.*, vol. 8, p. 298, May 2014.

[10] J. Powers, A. Wallace, A. Mansfield, G. Mochizuki, and K. K. Patterson, "The effect of frequency of feedback on overground temporal gait asymmetry post stroke," *Topics Stroke Rehabil.*, pp. 1–10, Jul. 2021.

[11] Y. Koyanagi *et al.*, "The effect of body weight-supported overground gait training for patients with Parkinson's disease: A retrospective case-control observational study," *PLoS ONE*, vol. 16, no. 7, Jul. 2021, Art. no. e0254415.

[12] C. Yoon-Hee, K. Kyoung, L. Sang-Yong, and C. Yong-Jun, "Lower limb muscle activities and gain in balancing ability following two types of stair gait intervention in adult post-chronic stroke patients: A preliminary, randomized-controlled study," *Turkish J. Phys. Med. Rehabil.*, vol. 66, no. 1, pp. 17–23, Mar. 2020.

[13] S. Hesse, C. Tomelleri, A. Bardeleben, C. Werner, and A. Waldner, "Robot-assisted practice of gait and stair climbing in nonambulatory stroke patients," *J. Rehabil. Res. Develop.*, vol. 49, no. 4, p. 613, 2012.

[14] I. Carpinella, E. Gervasoni, D. Anastasi, T. Lencioni, D. Cattaneo, and M. Ferrarin, "Instrumental assessment of stair ascent in people with multiple sclerosis, stroke, and Parkinson's disease: A wearable-sensor-based approach," *IEEE Trans. Neural Syst. Rehabil. Eng.*, vol. 26, no. 12, pp. 2324–2332, Dec. 2018.

[15] G. Puyuelo-Quintana *et al.*, "A new lower limb portable exoskeleton for gait assistance in neurological patients: A proof of concept study," *J. Neuroeng. Rehabil.*, vol. 17, no. 1, pp. 1–16, Dec. 2020.

[16] Z. F. Lerner, D. L. Damiano, H.-S. Park, A. J. Gravunder, and T. C. Bulea, "A robotic exoskeleton for treatment of crouch gait in children with cerebral palsy: Design and initial application," *IEEE Trans. Neural Syst. Rehabil. Eng.*, vol. 25, no. 6, pp. 650–659, Jun. 2017.

[17] H. Rezaie and M. Ghassemian, "An adaptive algorithm to improve energy efficiency in wearable activity recognition systems," *IEEE Sensors J.*, vol. 17, no. 16, pp. 5315–5323, Aug. 2017.

[18] E. Fullerton, B. Heller, and M. Munoz-Organero, "Recognizing human activity in free-living using multiple body-worn accelerometers," *IEEE Sensors J.*, vol. 17, no. 16, pp. 5290–5297, Aug. 2017.

[19] S. Gaglio, G. Lo Re, and M. Morana, "Human activity recognition process using 3-D posture data," *IEEE Trans. Human-Mach. Syst.*, vol. 45, no. 5, pp. 586–597, Oct. 2014.

[20] A. Wang, G. Chen, J. Yang, S. Zhao, and C.-Y. Chang, "A comparative study on human activity recognition using inertial sensors in a smartphone," *IEEE Sensors J.*, vol. 16, no. 11, pp. 4566–4578, Jun. 2016.

[21] Y. Zhang and Y. Ma, "Application of supervised machine learning algorithms in the classification of sagittal gait patterns of cerebral palsy children with spastic diplegia," *Comput. Biol. Med.*, vol. 106, pp. 33–39, Mar. 2019.

[22] H. Huang, F. Zhang, L. J. Hargrove, Z. Dou, D. R. Rogers, and K. B. Englehart, "Continuous locomotion-mode identification for prosthetic legs based on neuromuscular–mechanical fusion," *IEEE Trans. Biomed. Eng.*, vol. 58, no. 10, pp. 2867–2875, Oct. 2011.

[23] K. Zhang, M. Sun, D. K. Lester, F. X. Pi-Sunyer, C. N. Boozer, and R. W. Longman, "Assessment of human locomotion by using an insole measurement system and artificial neural networks," *J. Biomech.*, vol. 38, no. 11, pp. 2276–2287, 2005.

[24] S. E. Hussein and M. H. Granat, "Intention detection using a neuro-fuzzy EMG classifier," *IEEE Eng. Med. Biol. Mag.*, vol. 21, no. 6, pp. 123–129, Nov. 2002.

[25] M. Chen, J. Yan, and Y. Xu, "Gait pattern classification with integrated shoes," in *Proc. IEEE/RSJ Int. Conf. Intell. Robots Syst.*, Oct. 2009, pp. 833–839.

[26] U. Martínez-Hernandez and A. A. Dehghani-Sanij, "Adaptive Bayesian inference system for recognition of walking activities and prediction of gait events using wearable sensors," *Neural Netw.*, vol. 102, pp. 107–119, Jun. 2018.

[27] U. Martinez-Hernandez, I. Mahmood, and A. A. Dehghani-Sanij, "Simultaneous Bayesian recognition of locomotion and gait phases with wearable sensors," *IEEE Sensors J.*, vol. 18, no. 3, pp. 1282–1290, Feb. 2018.

[28] H. A. Varol, F. Sup, and M. Goldfarb, "Multiclass real-time intent recognition of a powered lower limb prosthesis," *IEEE Trans. Biomed. Eng.*, vol. 57, no. 3, pp. 542–551, Mar. 2010.

[29] A. G. Feldman, M. F. Levin, A. Garofolini, D. Piscitelli, and L. Zhang, "Central pattern generator and human locomotion in the context of referent control of motor actions," *Clin. Neurophysiol.*, vol. 132, no. 11, pp. 2870–2889, Nov. 2021.

[30] P. A. Guertin, "Central pattern generator for locomotion: Anatomical, physiological, and pathophysiological considerations," *Frontiers Neurol.*, vol. 3, p. 183, Feb. 2013.

[31] M. I. Jordan and T. M. Mitchell, "Machine learning: Trends, perspectives, and prospects," *Science*, vol. 349, no. 6245, pp. 255–260, 2015.

[32] C. L. Brockett and G. J. Chapman, "Biomechanics of the ankle," *Orthopaedics Trauma*, vol. 30, no. 3, pp. 232–238, 2016.

[33] H. Sadeghi, S. Sadeghi, F. Prince, P. Allard, H. Labelle, and C. L. Vaughan, "Functional roles of ankle and hip sagittal muscle moments in able-bodied gait," *Clin. Biomech.*, vol. 16, no. 8, pp. 688–695, Oct. 2001.

[34] A. J. Young, A. M. Simon, N. P. Fey, and L. J. Hargrove, "Intent recognition in a powered lower limb prosthesis using time history information," *Ann. Biomed. Eng.*, vol. 42, no. 3, pp. 631–641, 2014.

[35] N. U. Ahamed, D. Kobsar, L. C. Benson, C. A. Clermont, S. T. Osis, and R. Ferber, "Subject-specific and group-based running pattern classification using a single wearable sensor," *J. Biomech.*, vol. 84, pp. 227–233, Feb. 2019.

[36] J.-S. Wang, C.-W. Lin, Y.-T. C. Yang, and Y.-J. Ho, "Walking pattern classification and walking distance estimation algorithms using gait phase information," *IEEE Trans. Biomed. Eng.*, vol. 59, no. 10, pp. 2884–2892, Oct. 2012.

[37] A. Ferrari, P. Ginis, M. Hardegger, F. Casamassima, L. Rocchi, and L. Chiari, "A mobile Kalman-filter based solution for the real-time estimation of spatio-temporal gait parameters," *IEEE Trans. Neural Syst. Rehabil. Eng.*, vol. 24, no. 7, pp. 764–773, Jul. 2016.

[38] A. Anwary, H. Yu, and M. Vassallo, "An automatic gait feature extraction method for identifying gait asymmetry using wearable sensors," *Sensors*, vol. 18, no. 3, p. 676, Feb. 2018.

[39] R. Romijnders, E. Warmerdam, C. Hansen, J. Welzel, G. Schmidt, and W. Maetzler, "Validation of IMU-based gait event detection during curved walking and turning in older adults and Parkinson's disease patients," *J. Neuroeng. Rehabil.*, vol. 18, no. 1, pp. 1–10, Dec. 2021.

[40] J. C. Perez-Ibarra, A. A. G. Siqueira, and H. I. Krebs, "Identification of gait events in healthy and Parkinson's disease subjects using inertial sensors: A supervised learning approach," *IEEE Sensors J.*, vol. 20, no. 24, pp. 14984–14993, Dec. 2020.

[41] A. Schicketmueller, J. Lamprecht, M. Hofmann, M. Sailer, and G. Rose, "Gait event detection for stroke patients during robot-assisted gait training," *Sensors*, vol. 20, no. 12, p. 3399, Jun. 2020.

[42] A. R. Jimenez, F. Seco, J. C. Prieto, and J. Guevara, "Indoor pedestrian navigation using an INS/EKF framework for yaw drift reduction and a foot-mounted IMU," in *Proc. 7th Workshop Positioning, Navigat. Commun.*, Mar. 2010, pp. 135–143.

[43] A. R. J. Ruiz, F. S. Granja, J. C. P. Honorato, and J. I. G. Rosas, "Accurate pedestrian indoor navigation by tightly coupling foot-mounted IMU and RFID measurements," *IEEE Trans. Instrum. Meas.*, vol. 61, no. 1, pp. 178–189, Jan. 2012.

[44] A. Yassin *et al.*, "Recent advances in indoor localization: A survey on theoretical approaches and applications," *IEEE Commun. Surveys Tuts.*, vol. 19, no. 2, pp. 1327–1346, 2nd Quart., 2016.

[45] I. Skog, J.-O. Nilsson, and P. Händel, "Evaluation of zero-velocity detectors for foot-mounted inertial navigation systems," in *Proc. Int. Conf. Indoor Positioning Indoor Navigat.*, Sep. 2010, pp. 1–6.

[46] Y. Singh, V. Rodrigues, A. Prado, S. K. Agrawal, and V. Vashista, "Lower-limb strategy assessment during a virtual reality based dual-motor-task," in *Proc. 8th IEEE RAS/EMBS Int. Conf. Biomed. Robot. Biomechatronics (BioRob)*, Nov. 2020, pp. 252–257.

[47] S. R. Hundza *et al.*, "Accurate and reliable gait cycle detection in Parkinson's disease," *IEEE Trans. Neural Syst. Rehabil. Eng.*, vol. 22, no. 1, pp. 127–137, Jan. 2014.

[48] S. J. Lee and J. Hidler, "Biomechanics of overground vs. treadmill walking in healthy individuals," *J. Appl. Physiol.*, vol. 104, no. 3, pp. 747–755, Mar. 2008.